Originalarbeit

Berg Huettenmaenn Monatsh
https://doi.org/10.1007/s00501-022-01238-y

BHM Berg- und Hüttenmännische Monatshefte

Potential Causes for Cracking of a Laser Powder Bed Fused Carbon-free FeCoMo Alloy

Jan Platl[1], Daniel Rainer[1], Harald Leitner[2], Christoph Turk[2], Francesco Galbusera[3], Ali Gökhan Demir[3], Barbara Previtali[3], and Ronald Schnitzer[1]

[1]Department of Materials Science, Montanuniversität Leoben, Leoben, Austria
[2]voestalpine Böhler Edelstahl GmbH & Co KG, Kapfenberg, Austria
[3]Department of Mechanical Engineering, Politecnico di Milano, Milano, Italy

Received April 5, 2022; accepted April 26, 2022

Abstract: Compared to hot isostatic pressing or casting, laser-based powder bed fusion (LPBF) facilitates a near-net-shape fabrication of geometrically complex tools leading to a strongly reduced post-processing time and effort and consequently lower costs. Conventional tool steels are, however, prone to cracking during LPBF due to their high carbon equivalent numbers. In contrast, carbon-free maraging steels promise an enhanced processability due to the formation of a soft martensite, which is subsequently hardened by the precipitation of intermetallic phases.
A novel maraging steel for cutting applications (Fe25Co15Mo (wt%)) has been developed in recent years, and the present contribution deals with the processability of this novel alloy as a candidate for LPBF. However, severe cracking has been observed despite its low carbon content. The scanning electron microscopy revealed transcrystalline cleavage fracture plains on the crack surfaces. It is assumed that silicon oxide inclusions, which were verified by energy dispersive X-ray spectroscopy, are responsible for the brittle failure. The electron backscatter diffraction analysis revealed coarse elongated grains, which may also contribute to cracking. The differential scanning calorimetry could not confirm an influence of brittle ordered FeCo domains that are potentially formed during cooling. In conclusion, solution approaches for the fabrication of crack-free parts are presented.

Keywords: Laser powder bed fusion, Crack surface characterization, Maraging steel, Differential scanning calorimetry, Electron backscatter diffraction, FeCoMo alloy

Dr. J. Platl (✉)
Department of Materials Science,
Montanuniversität Leoben,
8700 Leoben, Austria
jan-platl@gmx.at

Potenzielle Rissursachen einer selektiv lasergeschmolzenen kohlenstofffreien FeCoMo Legierung

Zusammenfassung: Verglichen mit dem heißisostatischen Pressen oder dem Gießen ermöglicht das laserbasierte Pulverbettschmelzen (LPBF) eine endkonturnahe Fertigung geometrisch komplexer Werkzeuge, was zu einem stark reduzierten Nachbearbeitungsaufwand und folglich zu geringeren Kosten führt. Konventionelle Werkzeugstähle sind jedoch aufgrund ihres hohen Kohlenstoffäquivalents anfällig für Rissbildung während des LPBF-Prozesses. Im Gegensatz dazu versprechen kohlenstofffreie martensitische Stähle eine verbesserte Prozessierbarkeit aufgrund der Bildung eines weichen Martensits, der anschließend durch die Ausscheidung von intermetallischen Phasen ausgehärtet wird.
In den letzten Jahren wurde ein neuartiger martensitaushärtender Stahl für Zerspanungsanwendungen (Fe25Co15Mo (Gew.-%)) entwickelt. Der vorliegende Beitrag befasst sich mit der Verarbeitbarkeit dieser neuen Legierung als potenzielle Legierung für LPBF. Trotz des geringen Kohlenstoffgehalts wurde eine ausgeprägte Rissbildung beobachtet. Die Rasterelektronenmikroskopie zeigte transkristalline Spaltbruchebenen auf den Rissflächen. Es wird angenommen, dass Siliziumoxideinschlüsse, die durch energiedispersive Röntgenspektroskopie nachgewiesen wurden, für die beobachteten Sprödbruche verantwortlich sind. Mikrostrukturuntersuchungen mittels Elektronenrückstreubeugung zeigten grobe, längliche Körner, die ebenfalls zur Rissbildung beitragen können. Die dynamische Differenzkalorimetrie konnte einen Einfluss von spröden, geordneten FeCo-Domänen, die sich möglicherweise beim Abkühlen bilden, nicht bestätigen. Abschließend werden potenzielle Lösungsansätze für die Herstellung von rissfreien Teilen vorgestellt.

Schlüsselwörter: Selektives Laserschmelzen, Rissflächencharakterisierung, Maragingstahl, Dynamische Differenzkalorimetrie, Elektronenrückstreubeugung, FeCoMo Legierung

1. Introduction

Besides numerous other industry sectors, tooling is a very promising application field of additive manufacturing (AM) [1]. With regard to cutting applications such as drills or milling cutters, the implementation of internal cooling channels via LPBF could significantly improve productivity by enabling higher cutting velocities [2]. In addition, the high accuracy and the layer-by-layer nature of the process facilitate a significant reduction of the post-processing effort due to the possibility to manufacture near-net-shaped parts. Concerning small to medium lot sizes accompanied by large design variety of these tools, LPBF is also appealing for a reduction of the lead times and production costs [3]. As conventional maraging steels (e.g. 17-4PH, 15-5PH and 18Ni300), which promise good processability with LPBF, do not exhibit a sufficiently high hardness, high-carbon containing tool steels are conventionally used for cutting applications. However, these cold-work tool or high-speed steels are prone to cracking during LPBF due to their high carbon equivalent numbers. To account for this issue, novel alloying systems have to be considered.

Back in 1932, Köster [4] already said that martensitic FeCoMo alloys are generally capable of reaching a Rockwell hardness level of 70 HRC. This is guaranteed by precipitation hardening, which can be compared to that of conventional maraging steels. Instead of precipitating intermetallic Ni, Ti, or Al containing phases from a supersaturated FeNi martensite, these alloys gain their high hardness through the precipitation of nm-sized μ-phases ($(Fe,Co)_7Mo_6$) from a Mo supersaturated FeCo martensite.

A typical representative for this alloying group, which is used in industrial cutting applications (e.g. as hobbing cutter), is the Fe25Co15Mo (by weight) alloy. Preliminary investigations of this alloy fabricated via LPBF showed that the as-built state directly after the process guarantees a highly supersaturated state that can be compared to the conventional material's condition after solution annealing with subsequent quenching. Heat treatment variations revealed that, from this highly supersaturated FeCoMo martensite, nm-sized μ-phase particles are precipitated after a single ageing treatment for 3 h at approx. 600 °C with subsequent air cooling. Compared to a hardness of ~40 HRC in the as-built state, this heat treatment yielded ~70 HRC, which can be compared to the hardness potential of the conventionally manufactured material in fully heat-treated condition according to Danninger et al. [5].

Based on the extraordinarily high hardness, this alloy possesses a great potential for tooling applications. However, a well-known phenomenon that promotes failure of conventionally manufactured FeCoMo alloys is the formation of ordered FeCo domains. Zhao et al. [6] investigated FeCo alloys and concluded that the formation of ordered domains deteriorates the elongation to zero for Fe30Co and Fe50Co (at%). A similar behavior was found by Turk et al. [7, 8], who revealed a significant reduction in impact toughness of a Fe25Co15Mo (wt%) alloy after overaging during which almost the entire Mo had been removed from the matrix by diffusion processes resulting in the formation of μ-phases. This toughness decrease can also be attributed to the formation of ordered FeCo domains during slow cooling of the remaining Fe29Co (at%) matrix.

It is reasonable to assume that this FeCoMo maraging steel can be easily processed by LPBF due to the lack of carbon. However, the abovementioned preliminary study showed that, irrespective of the chosen process parameters, severe cracking occurs during the LPBF processing. Therefore, the macro- and microscopic crack appearance has been investigated and special attention was paid to the crack surface characterization using scanning electron microscopy (SEM). This contribution aims to illuminate potential causes for the observed cracking behavior. Hence, different characterization methods were carried out in order to evaluate potential cracking causes. Firstly, a differential scanning calorimetry (DSC) has been used to study precipitation reactions and the potential occurrence of brittle ordered domains. Secondly, the grain structures, which may contribute to crack formation, have been characterized using electron backscatter diffraction (EBSD). Thirdly, an energy dispersive X-ray spectroscopy (EDX) on the crack surface was used to analyze non-metallic inclusions that may cause crack formation during LPBF.

2. Investigated Material and Used Methods

A spherically shaped carbon-free steel powder with a composition (by weight) of Fe25Co15Mo was Argon gas atomized and subsequently sieved by voestalpine Böhler Edelstahl GmbH & Co KG, Kapfenberg, to the desired powder grain size of 15–45 μm.

In order to investigate the processability of this alloy with LPBF, samples with a base area of $10 \times 10\,mm^2$ and corresponding heights of 10, 50, 100, 150, 200, 300, 400, and 500 layers (layer thickness = 40 μm) were manufactured using a Renishaw AM250 machine fitted with a reduced build platform. The sample fabrication was carried out on a mild steel build platform. No platform preheating was used to constrain the energy input to the laser irradiation. An energy input of ~59 J/mm³ was chosen. The latter can be calculated based on the chosen process parameters by using the volumetric energy density *VED* according to Eq. 1 [9].

$$VED = \frac{\text{laser power} \cdot \text{pulse duration}}{(\text{point distance} \cdot \text{hatch distance} \cdot \text{layer thickness})} = \frac{250\,W \cdot 80\,\mu s}{(0.065\,mm \cdot 0.104\,mm \cdot 0.04\,mm)} \quad (1)$$

A light optical microscopy (LOM, Zeiss Axio Imager M1m) was carried out on cross-sectional polishes to characterize the defect structure of the samples. Special attention was paid to two samples with 100 and 500 layers, respectively. These samples were cut in the middle, grinded,

and polished with diamond suspension down to 1 µm with a final polishing step using the Struers oxide polishing suspension (OPS). The crack surface characterization was conducted using a Tescan Clara scanning electron microscope (SEM) in secondary (SE) and backscattered electron (BSE) detection mode at a working distance of 10 mm. Energy dispersive X-ray spectroscopy (EDX) spot measurements were carried out with an acceleration voltage of 10 kV in the same device in combination with the X-Max system and the corresponding Aztec software from Oxford Instruments.

The electron backscatter diffraction (EBSD) analysis was performed in a Versa 3D SEM from FEI on the sample with 100 layers. This device is equipped with a Hikari EBSD system from EDAX. For the EBSD mapping (458 × 357 µm^2, step size: 0.25 µm), an acceleration voltage of 20 kV at a working distance of 10 mm was chosen. The electrolytical polishing was carried out on a Struers Lectropol machine with the same polishing parameters as used by Turk et al. [10] after mechanical grinding and polishing to guarantee a deformation free surface. The data evaluation has been performed using EDAX orientation imaging microscopy (OIM) analysis software package (version 7). Apart from an inverse pole figure (IPF) map, a grain orientation spread (GOS) has been used to depict a potential epitaxial grain orientation with respect to the horizontal axis of the scan.

For the calculation of grain sizes, the assumption of perfectly elliptical grains has been made. Grain statistics from the software yielded values for the aspect ratio *AR* that are calculated according to Eq. 2.

$$AR = \frac{\text{minor axis}}{\text{major axis}} = \frac{d_{\min}}{d_{\max}} \tag{2}$$

By taking the area formula of an ellipsis $A = (d_{\min} \cdot d_{\max} \cdot \pi)/4$ into account, Eqs. 3 and 4 can be used to determine the mean minor (d_{min}) and major grain axis (d_{max}), respectively

$$d_{\min} = \sqrt{\frac{4 \cdot A \cdot AR}{\pi}} \tag{3}$$

$$d_{\max} = \sqrt{\frac{4 \cdot A}{AR \cdot \pi}} \tag{4}$$

To analyze the potential occurrence of ordered domains, a differential scanning calorimetry (DSC) was used. The experiments were conducted on a Setaram Labsys DSC, in which the specimens were heated to 800 °C with two different heating rates of 5 K/min and 20 K/min, respectively. Al2O3 was used as crucible material in a dynamic argon atmosphere with a flow rate of 20 ml/min. Four different conditions were analyzed. As-received powder (~ 100 mg) was investigated without any further preparation. The latter and an AM sample in the as-built condition were compared to conventionally manufactured material (soft-annealed), which was selectively heat treated to guarantee (slow cooled SC sample) or to avoid (water quenched WQ sample) the formation of the brittle ordered phase described above. The heat treatment procedures for the SC and WQ samples were taken from [8] and are as follows:

- SC to guarantee ordering: solution annealing at 800 °C for 30 min with three subsequent slow furnace cooling steps:
  - 800 to 600 °C with a rate of 0.5 K/min,
  - 600 to 500 °C with a rate 0.083 K/min,
  - 500 °C to room temperature with a rate of 0.5 K/min.
- WQ to avoid ordering: solution annealing at 800 °C for 30 min with subsequent water quenching.

These three samples (AM, SC, and WQ), were cut and subsequently grinded to a dimension of ~ 2 × 2 × 3.5 mm^3 and consequently possessed a mass of ~ 100 mg.

3. Results and Discussion

3.1 Macroscopic Crack Appearance and Surface Characterization

Fig. 1a shows an overview of the fabricated specimens. At this macroscopic level, the occurrence of cracks or delaminations cannot be deduced. Hence, LOM micrographs of

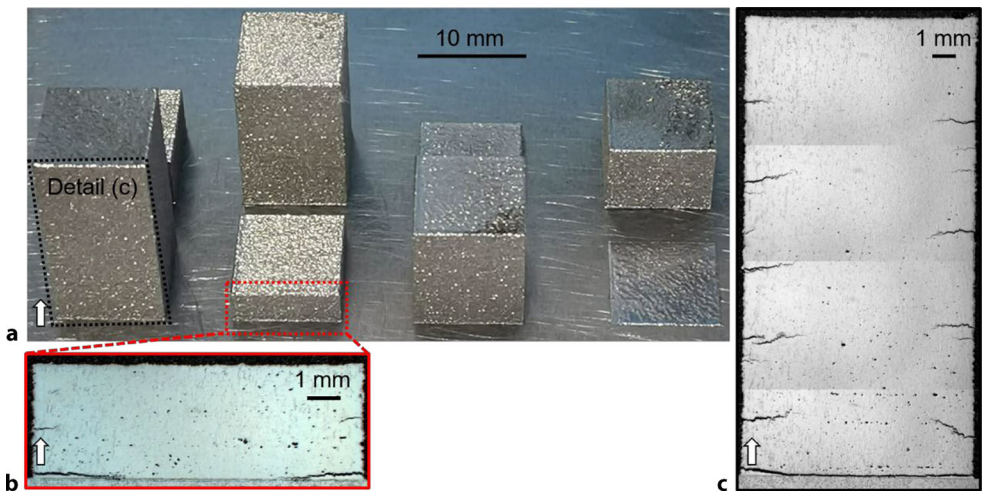

Fig. 1: **a** Macroscopic specimen overview. LOM micrographs of specimens with **b** 100 layers, and **c** 500 layers. It can be seen that cracks start from the transition zone to the building platform and from sample edges. The *white arrows* mark the building direction

samples with 100 layers and 500 layers are depicted in Fig. 1b and c, respectively. These cross-sections exhibit cracks, which initiate from the edges of the samples, and also the presence of a delamination between AM sample and build platform at the bottom of the micrographs is obvious. Additionally, Fig. 1c shows that all cracks propagate almost perpendicular to the build direction, which is indicated by the *white symbols* in the left bottom corner of the micrograph.

A regular arrangement of the cracks can be seen in both samples. This regularity indicates stress accumulations, which lead to the formation of the observed cracks. In a recent work [11], we determined similar stress accumulations by means of strain profile measurements using synchrotron radiation. These accumulations are responsible for crack formation of a LPBF carbon-containing cold-work tool steel. As the manufacturing process is identical, the investigated alloy may also have failed through process-related thermal stresses in the tensile regime at the sample edge.

Fig. 2 depicts an exemplary SEM fractograph of the crack surface. Based on its morphology, the failure mode can be clearly assigned as brittle transcrystalline cleavage fracture.

In order to shed light on the potential causes for this transcrystalline cleavage fracture, well-known reasons for brittle material failure and material-specific influence factors were taken into account in the following section. In terms of the latter, the formation of ordered FeCo domains, which basically promotes brittle failure of conventionally manufactured FeCoMo alloys, was investigated by means of DSC measurements. This technique additionally facilitates the analysis of precipitation reactions, which may also play a role in cracking. Basically, coarse grains may deteriorate the ductility of metals, which may possibly contribute to brittle failure. Therefore, EBSD has been carried in order to evaluate the grain size and orientation that evolves during LPBF. Lastly, non-metallic inclusions may trigger brittle failure in metals. Their potential occurrence on the crack surface has been investigated with SEM and their chemical composition has been qualitatively evaluated using EDX.

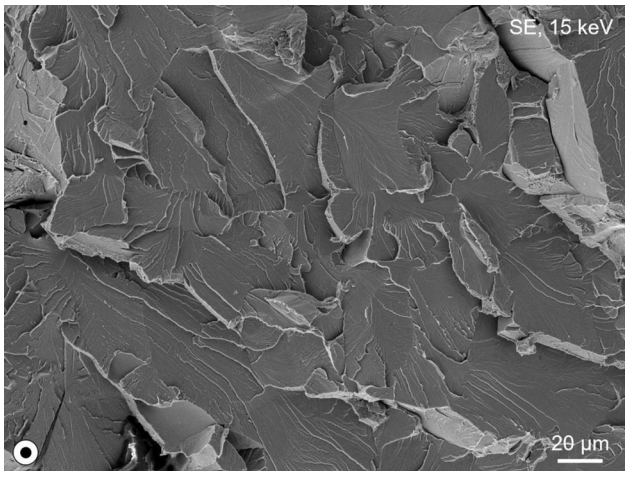

Fig. 2: Exemplary SEM fractograph showing transcrystalline cleavage fracture. The *white symbol* marks the building direction

4. Potential Cracking Reasons

The occurrence of brittle ordered domains has been investigated as a first possible reason for the observed cleavage fracture. Therefore, DSC heating experiments were conducted in accordance with investigations performed by Turk et al. [12]. Special attention was paid to the heat flow at a temperature of ~590 °C [13], at which a disordering peak should emerge if the material contains ordered domains. Fig. 3a and b depict typical DSC curves, in which the heat flow is plotted as a function of the sample temperature, for the two heating rates of 5 K/min and 20 K/min, respectively. It can be clearly seen in Fig. 3b that the endothermal ordering peak (I) at a temperature of 590 °C only exists in the conventionally manufactured slow cooled (SC) sample.

This can be explained because this ordering process requires a certain amount of time, which cannot be guaranteed if the material is quenched too rapidly. Although LPBF is characterized by extremely rapid cooling conditions, the formation of these brittle ordered phases could have been possible during in-situ tempering processes by layers welded on the already existing ones. However, the conventionally manufactured and rapidly quenched (WQ) reference sample, the powder, and the AM sample exhibit no such endothermal disordering peak. Therefore, it can be concluded that no disordering process has occurred because no ordered domains were present in the starting condition (i.e. as-built state of the AM sample) at the beginning of the DSC experiment. Consequently, the formation of brittle ordered domains is not likely to cause the transcrystalline material failure of the LPBF samples.

Furthermore, the conducted DSC measurements provide information about possible precipitation reactions. From Fig. 3a, it can be deduced that, apart from the endothermal ordering peak, no further peaks and consequently no precipitation reactions are obvious during heating of the SC sample. This can be explained because overaging at 800 °C with subsequent furnace cooling results in a pure FeCo matrix from which no Mo could be precipitated as it has already been incorporated in µ-phase formation. In contrast, the three remaining samples comprise a FeCo matrix, that is highly supersaturated in Mo due to rapid cooling rates. All depict the presence of peak (II) at temperatures ranging from 500 to 560 °C. This peak can possibly be attributed to a Mo diffusion and clustering process, which was also observed for the same material in conventionally manufactured condition by Leitner et al. [21]. Peaks (III) and (IV) are obvious in Fig. 3b for the powder and the AM sample. Those can be assigned to the formation and subsequent coarsening of the µ-phase and are again in good agreement with investigations performed for the same alloy in conventionally manufactured condition [14, 15]. No clear statements about the role of precipitates in cracking can be drawn solely from these DSC experiments. Their detailed investigation will be the subject of future studies.

Fig. 4a shows the inverse pole figure (IPF) color map, which was determined using EBSD on the electropolished surface, of a sample with 100 layers. The *white arrow* in the bottom left corner marks the build direction during

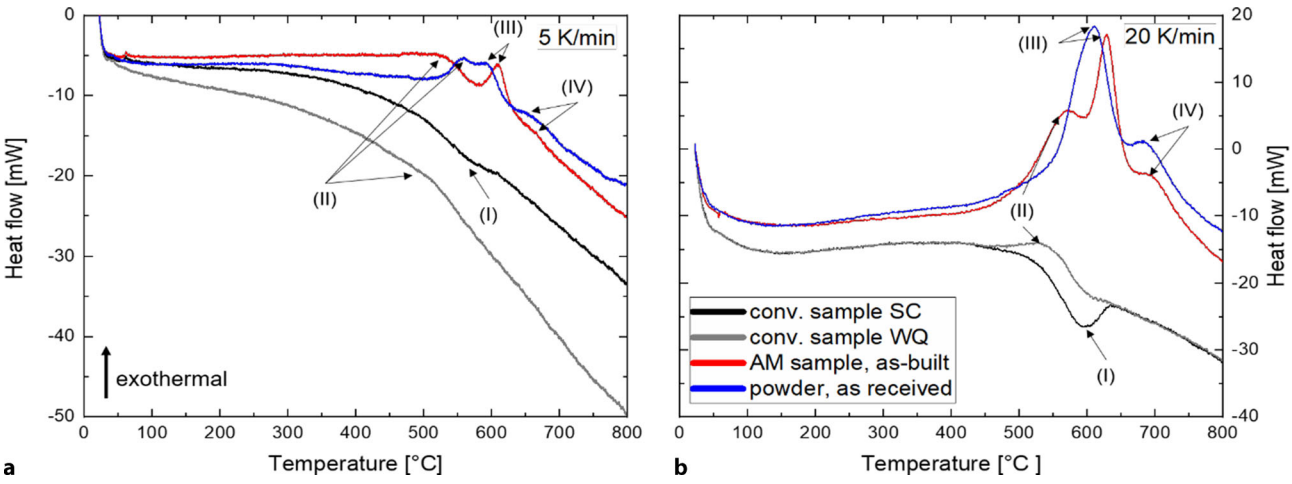

Fig. 3: DSC curves for different sample conditions at heating rates of **a** 5 K/min and **b** 20 K/min. Peak (I) only emerges during heating of the conventionally manufactured slow cooled (SC) sample. Zero lines have been subtracted

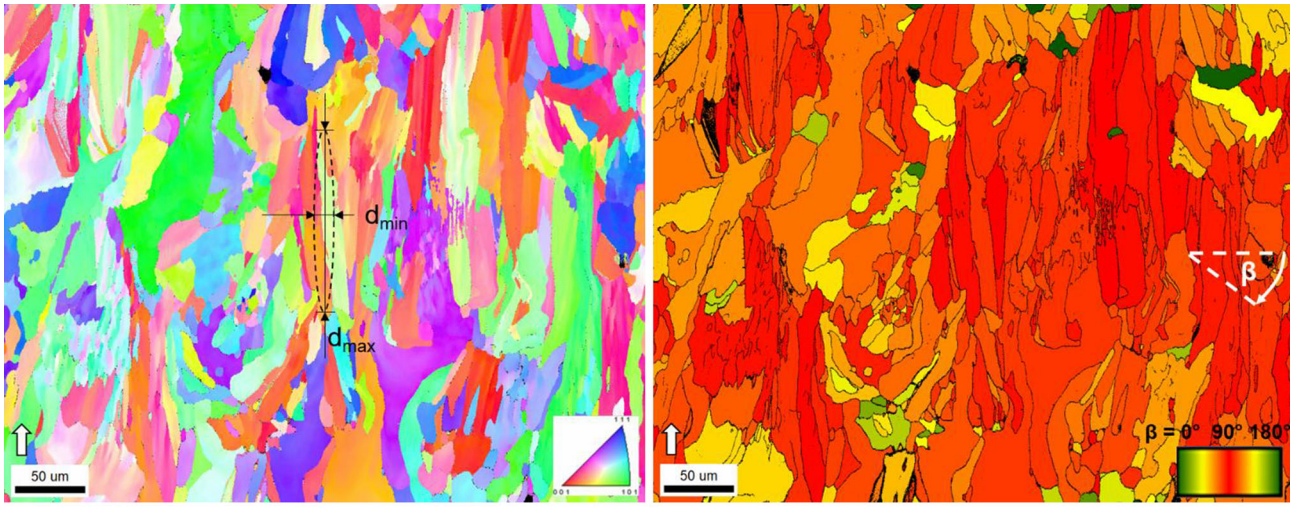

Fig. 4: **a** IPF color map for bcc phase with calculated d_{min} = 19.2 µm and d_{max} = 86.5 µm. **b** GOS map depicting a strong epitaxial grain growth. The *white symbols* mark the building direction

LPBF. More than 99% of the area have been indicated as a body-centered cubic (bcc) phase. Therefore, the as-built microstructure is highly likely to consist of a Mo-supersaturated FeCo martensite that formed during rapid cooling. It can be seen that most grains are elongated in build direction. By taking into account the chosen layer thickness of 40 µm, it can be concluded that grain growth occurs towards several layers.

In order to estimate the minimum and maximum grain diameters, as described in the methods section, the following averaged values for the grain area and the aspect ratio were extracted from the EBSD data plots of the grain area and the aspect ratio, both in dependence of the cumulative area fraction: $A_{50\%}$ = 1303 µm^2 and $AR_{50\%}$ = 0.22. By inserting these values in Eqs. 3 and 4, the mean diameters amount to d_{min} = 19.2 µm and d_{max} = 86.5 µm, respectively. Basically, coarse grains often contribute to brittle failure of steels because of the higher ductile-brittle transition temperatures [16]. The calculated values for d_{min} and d_{max} are relatively large in comparison to other investigations of AM maraging steels. Tan et al. [17] also evaluated the grain size with EBSD of a LPBF grade 300 maraging steel and concluded a mean grain diameter of 0.31 µm. Similar experiments were conducted by Mutua et al. [18], who also found a mean grain size below 1 µm.

Fig. 4b depicts the same scan but as a map of the grain orientation spread (GOS). This illustration shows the orientation of grains through the angle β relative to the horizontal axis. It can be seen that the majority of the grains is depicted in red and orange and these grains are therefore oriented almost parallel to the build direction. Hence, a strong epitaxial grain orientation is obvious. These epitaxial structures can be explained by the nature of the AM process [19].

In terms of cracking, no correlation between grain orientation and crack propagation was found as the failure occurred in a transcrystalline manner. Due to the relatively coarse grain structures, which were found using EBSD,

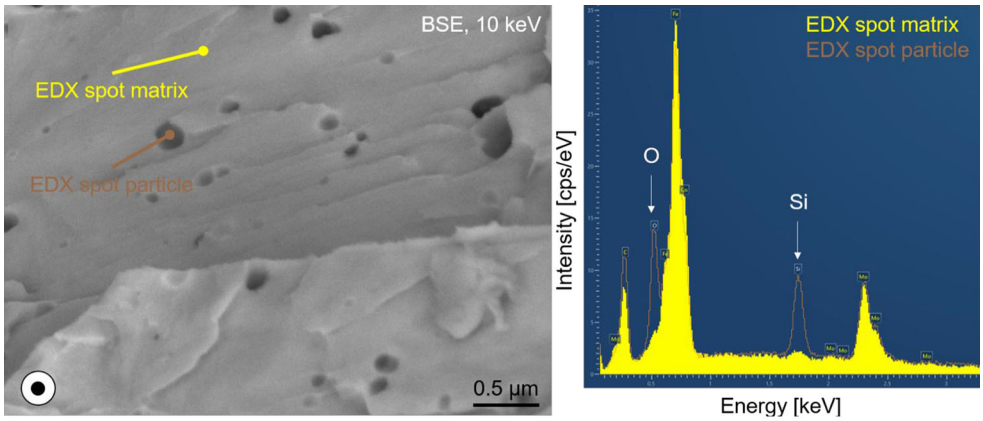

Fig. 5: **a** BSE SEM fractograph with corresponding **b** qualitative EDX spot spectra of matrix and particle composition. The latter can be clearly assigned to silicon oxide. The *white symbol* in **a** marks the building direction

a significant contribution to cracking is possible. In order to avoid a coarsening during LPBF, Zhang et al. [20] investigated the influence of different *VED*s on the grain structure of commercially pure titanium. This approach could also result in significant grain refinement and thus in a possible improvement of crack resistance of the investigated FeCoMo alloy. The change of *VED* may also alter the porosity of the produced material, as too low levels would generate lack-of-fusion while too high levels can induce keyhole porosity. The control of laser power profile temporally and spatially may provide further flexibility [21–23].

Non-metallic inclusions are often responsible for the failure of steels as they represent potential sites for stress concentrations [24]. In a hard and therefore relatively brittle material such as the investigated FeCoMo alloy, these inclusions may serve as starting points for transcrystalline failure. Therefore, special attention has been paid to the possible occurrence of non-metallic inclusions on the crack surface.

Fig. 5a shows a high resolution BSE SEM fractograph, in which a transcrystalline cleavage failure can be seen (cf. Fig. 2d). The presence of dark spherically shaped phases with dimensions below 300 nm is obvious. As darker depicted structures in the BSE mode comprise lighter elements, the presence of oxides was assumed. Evidence of their presence on the crack surface is given by the EDX spot measurements depicted in Fig. 5b. A comparison of the matrix spot and the particle spot clearly assigns these non-metallic inclusions as silicon oxides.

These Si-rich inclusions probably formed due to the presence of residual oxygen during atomization or in the Argon gas atmosphere of the LPBF process. This assumption is in accordance with an investigation of a LPBF 316L steel published by Zhong et al. [25]. In order to reduce the risk of cracking due to such Si-rich non-metallic inclusions, a promising approach would be to atomize a powder without Si additions as this element is not mandatory for the mechanical performance (i.e. hardness level) of the investigated alloy.

Out of the potential cracking reasons discussed above, the presence of silicon oxides on the crack surface is the one with the highest probability of causing the failure of the investigated FeCoMo alloy. As a further potential cracking source, the formation of precipitates during LPBF should be mentioned. Due to the precipitation of potentially brittle phases, the observed transcrystalline failure may be promoted. In order to characterize this potential impact factor on cracking, high resolution techniques such as atom probe tomography or transmission electron microscopy would be necessary.

5. Conclusions

The present contribution aimed to illuminate the potential cracking causes of a Fe25Co15Mo alloy. Despite this alloy promising a good processability with LPBF, severe cracking has been observed. In order to characterize the crack surface, SEM investigations were performed. A DSC analysis has been conducted to shed light on the potential formation of ordered domains. Furthermore, the grain structure has been investigated using EBSD. Lastly, EDX spot measurements were carried out to analyze non-metallic inclusions on the crack surface. From the obtained results, the following conclusions and potential remedial measures can be drawn for the different potential cracking reasons:

The macroscopic crack appearance has been investigated using LOM and revealed a regular arrangement of cracks that initiate from geometrically notched positions such as the transition between AM material and build platform or the sample edges. This regularity suggests the presence of stress accumulations that evolve during LBPF and cause cracking. In order to reduce the thermal gradient and consequently to decrease the stress level beneath the material's rupture strength during LPBF, the build platform could be preheated. The crack surface morphology in the SEM clearly displayed a transcrystalline cleavage fracture. For this failure mode, three potential sources were discussed.

The potential occurrence of brittle ordered domains has been investigated with DSC. Results clearly revealed that, due to rapid cooling processes during LPBF and consequently high Mo supersaturation, no ordered FeCo domains were formed. Hence, no correlation between these ordered domains and the crack occurrence could be drawn.

No relation between grain structure and crack formation was found with the EBSD investigations. However, the relatively large grain size compared to other LBPF materials may contribute to cracking. In-situ grain refinement could be possible by variations of the LPBF process parameters.

The occurrence of non-metallic inclusions was determined as the most probable cause for cracking. EDX spot measurements clearly revealed that these inclusions comprise Si and O. Because a further reduction of O contamination during atomization and LPBF is hard to realize, a promising approach to avoid the formation of these silicon oxides is to remove Si from the powder. The latter is not mandatory for the mechanical performance of the investigated FeCoMo alloy.

Acknowledgements. Funding from the Austrian BMK (846933) in the framework of the program "Production of the future" and the "BMK Professorship for Industry" is gratefully acknowledged. The Italian Ministry of Education, University and Research is acknowledged for the support provided through the Project "Department of Excellence LIS4.0—Lightweight and Smart Structures for Industry 4.0".

Funding. Open access funding provided by Montanuniversität Leoben.

References

1. Gibson, I., Rosen, D., Stucker, B.: Additive manufacturing technologies. Springer, New York (2015)
2. Sander, J., Hufenbach, J., Giebeler, L., Wendrock, H., Kühn, U., Eckert, J.: Microstructure and properties of FeCrMoVC tool steel produced by selective laser melting. Mater Des **89**, 335–341 (2016)
3. Previtali, B., Demir, A.G., Crosato, A., Penasa, M.: Comparative costs of additive manufacturing vs. machining: the case study of the production of forming dies for tube bending. 28th Annual International Solid Freeform Fabrication Symposium—An Additive Manufacturing Conference August, Austin., pp. 7–9 (2017)
4. Köster, W.: Mechanische und magnetische Ausscheidungshärtung der Eisen-Kobalt-Wolfram-und Eisen-Kobalt-Molybdän-Legierungen. Arch. Eisenhüttenwes. **6**, 17–23 (1932)
5. Danninger, H., Rouzbahani, F., Harold, C., Ponemayr, H., Daxelmuller, M., Simancik, F., Izdinsky, K.: Heat treatment and properties of precipitation hardened carbon-free PM tool steels. Powder Met. Prog **5**, 92–103 (2005)
6. Zhao, L., Baker, I.: The effect of grain size and Fe: Co ratio on the room temperature yielding of FeCo. Acta Met. Mater **42**, 1953–1958 (1994)
7. Turk, C., Leitner, H., Schemmel, I., Clemens, H., Primig, S.: Atom probe study of B2 order and A2 disorder of the FeCo matrix in an Fe-Co-Mo-alloy. Micron **98**, 24–33 (2017)
8. Turk, C., Leitner, H., Kellezi, G., Clemens, H., Gan, W.M., Staron, P., Primig, S.: Impact of the B2 ordering behavior on the mechanical properties of a FeCoMo alloy. Mater. Sci. Eng. A **662**, 511–518 (2016)
9. Kruth, J.-P., Kumar, S., Van Vaerenbergh, J.: Study of laser-sinterability of ferro-based powders. Rapid Prototyp J **11**, 287–292 (2005)
10. Turk, C., Kellezi, G., Leitner, H., Clemens, H., Primig, S.: Influence of the sample preparation technique on the μ phase fraction analysis in a Fe-25Co-15Mo alloy by means of XRD. Pract. Met. **52**, 323–333 (2015)
11. Platl, J., Bodner, S., Hofer, C., Landefeld, A., Leitner, H., Turk, C., Nielsen, M.-A., Demir, A.G., Previtali, B., Keckes, J., Schnitzer, R.: Cracking mechanism in a laser powder bed fused cold-work tool steel: The role of residual stresses, microstructure and local elemental concentrations. Acta Mater **225**, 117570 (2022)
12. Turk, C., Kellezi, G., Leitner, H., Staron, P., Gan, W., Clemens, H., Primig, S.: B2 order transformation in a Fe–25 at% Co–9 at% Mo alloy. Mater. Res. Soc. Symp. Proc. **1760**, 175–180 (2014). https://doi.org/10.1557/opl.2015.117
13. Nishizawa, T., Ishida, K.: The Co– Fe (Cobalt– Iron) system. Bull. Alloy. -ph. Diagrams **5**, 250 (1984)
14. Leitner, H., Schober, M., Clemens, H., Caliskanoglu, D., Danoix, F.: Precipitation behaviour of an Fe–Co–Mo-alloy during non-isothermal ageing. Int. J. Mater. Res. **99**, 367–374 (2008)
15. Eidenberger, E., Schober, M., Schmoelzer, T., Stergar, E., Staron, P., Leitner, H., Clemens, H.: Analysis of the multistage phase separation reaction in Fe–25 at% Co–9 at% Mo. Phys. Status Solidi A **207**, 2238–2246 (2010)
16. Morris, J.W.J.R.: Proceedings of the International Symposium on Ultrafine Grained Steels September 20–22. Tokyo. Iron and Steel Institute of Japan, Tokyo (2001)
17. Tan, C., Zhou, K., Kuang, M., Ma, W., Kuang, T.: Microstructural characterization and properties of selective laser melted maraging steel with different build directions. Sci. Technol. Adv. Mater. **19**, 746–758 (2018)
18. Mutua, J., Nakata, S., Onda, T., Chen, Z.-C.: Optimization of selective laser melting parameters and influence of post heat treatment on microstructure and mechanical properties of maraging steel. Mater Des **139**, 486–497 (2018)
19. Basak, A., Das, S.: Epitaxy and microstructure evolution in metal additive manufacturing. Annu. Rev. Mater. Res. **46**, 125–149 (2016)
20. Zhang, J., Liu, Y., Bayat, M., Tan, Q., Yin, Y., Fan, Z., Liu, S., Hattel, J.H., Dargusch, M., Zhang, M.-X.: Achieving high ductility in a selectively laser melted commercial pure-titanium via in-situ grain refinement. Scripta Mater. **191**, 155–160 (2021)
21. Demir, A.G., Mazzoleni, L., Caprio, L., Pacher, M., Previtali, B.: Complementary use of pulsed and continuous wave emission modes to stabilize melt pool geometry in laser powder bed fusion. Opt. Laser. Technol. **113**, 15–26 (2019)
22. Demir, A.G., Previtali, B.: Investigation of remelting and preheating in SLM of 18Ni300 maraging steel as corrective and preventive measures for porosity reduction. Int. J. Adv. Manuf. Techn. **93**, 2697–2709 (2017)
23. Catchpole-Smith, S., Aboulkhair, N., Parry, L., Tuck, C., Ashcroft, I.A., Clare, A.: Fractal scan strategies for selective laser melting of 'unweldable' nickel superalloys. Addit. Manuf. **15**, 113–122 (2017)
24. Park, J.H., Kang, Y.: Inclusions in stainless steels—a review. Steel Res. Int. **88**, 1700130 (2017)
25. Zhong, Y., Liu, L., Wikman, S., Cui, D., Shen, Z.: Intragranular cellular segregation network structure strengthening 316L stainless steel prepared by selective laser melting. J. Nucl. Mater. **470**, 170–178 (2016)